Through-Thickness Residual Stress Profiles in Austenitic Stainless Steel Welds: A Combined Experimental and Prediction Study

Through-Thickness Residual Stress Profiles in Austenitic Stainless Steel Welds: A Combined Experimental and Prediction Study

J. MATHEW, R.J. MOAT, S. PADDEA, J.A. FRANCIS, M.E. FITZPATRICK, and P.J. BOUCHARD

Economic and safe management of nuclear plant components relies on accurate prediction of welding-induced residual stresses. In this study, the distribution of residual stress through the thickness of austenitic stainless steel welds has been measured using neutron diffraction and the contour method. The measured data are used to validate residual stress profiles predicted by an artificial neural network approach (ANN) as a function of welding heat input and geometry. Maximum tensile stresses with magnitude close to the yield strength of the material were observed near the weld cap in both axial and hoop direction of the welds. Significant scatter of more than 200 MPa was found within the residual stress measurements at the weld center line and are associated with the geometry and welding conditions of individual weld passes. The ANN prediction is developed in an attempt to effectively quantify this phenomenon of 'innate scatter' and to learn the non-linear patterns in the weld residual stress profiles. Furthermore, the efficacy of the ANN method for defining through-thickness residual stress profiles in welds for application in structural integrity assessments is evaluated.

DOI: 10.1007/s11661-017-4359-4

I. INTRODUCTION

FUSION welding continues to be the most practical fabrication technique for joining heavy section steel components in piping systems used in the power generation and petrochemical industries. Welding introduces high-magnitude tensile residual stresses in the vicinity of the weld zone, causing cracks to initiate and grow in service.[1] Fitness-for-service assessment of welded components containing defects must take account of residual stresses remaining in the welded joint as well as the applied service loading conditions.[2] Several measurement techniques are reported[3] that can be employed to quantify the magnitude and distribution of residual stress in welds, for example those based on diffraction or mechanical strain-relief methods. In general, neutron diffraction[4] and the contour method[5] can be used to map the distribution of residual stress in austenitic stainless steel piping components. Such measured data can be applied directly in fracture assessments, or used to validate finite element models based on weld mechanics.

Welding-induced residual stress simulated using the finite element method can be largely dependent on modeling approach, constitutive model, and material properties used by the analyst.[6] Recent developments in the capabilities of measurement techniques and improved corroboration between measurements made using diverse methods have created the opportunity to develop data-based models for predicting residual stress in weldments based on experimental measurements. For example, through-thickness residual stress distribution were compared to good effect using neutron diffraction, contour method, and deep hole drilling in low- and high-heat-input welds.[7]

Undertaking residual stress measurements in welds can be quite challenging. Neutron diffraction is being increasingly used to map residual stresses in weldments to depths of several millimeters. However, acquiring reliable stress-free reference parameters in multi-pass austenitic stainless steel welds can be challenging owing to compositional variations, texture, and inter-granular

J. MATHEW is with the Faculty of Engineering and Computing, Coventry University, Priory Street, Coventry, CV1 5FB also with the Department of Engineering and Innovation, The Open University, Walton Hall, Milton Keynes, MK7 6AA, UK. Contact e-mail: Jino.Mathew@coventry.ac.uk R.J. MOAT, S. PADDEA, and P.J. BOUCHARD are with the Department of Engineering and Innovation, The Open University, Walton Hall, Milton Keynes, MK7 6AA, UK. M.E. FITZPATRICK is with the Faculty of Engineering and Computing, Coventry University, Priory Street, Coventry, CV1 5FB, UK. J.A. FRANCIS is with the School of Mechanical, Aerospace and Civil Engineering, University of Manchester, Manchester, M13 9PL, UK

Manuscript submitted January 25, 2017.
Article published online October 5, 2017

stresses.[8] The contour method is a destructive technique that can map residual stresses acting normal to a selected cut plane. The method has been successfully applied to a range of welded components, although the reliability of the measurement is highly dependent on the quality of the cut.[9,10] Greater confidence in measured residual stresses can be obtained by using neutron diffraction and the contour method in tandem. However, the phenomenon of innate scatter of residual stress fields in welds[11] makes characterisation of residual stresses to known confidence level an arduous task.

Artificial neural networks (ANNs)[12] are abstract models consisting of processing elements called neurons that have the ability to generalize patterns associated with non-linear systems. The rationale for using ANN is the ability to map input-output relationships where analytical solutions are unavailable or too complex to develop. A multi-layer perceptron (MLP) is a typical ANN architecture with an input layer, output layer, and an intermediate layer described as the 'hidden layer' between the input and output layers. ANNs within a Bayesian framework have been successfully applied in a broad range of problems in material science.[13] In recent years, attempts have been made to predict through-thickness residual stresses using ANNs and other data-based models.[14,15] However, an ANN approach has not been applied to measured weld residual stress data despite the fact that several parameterised models based on the finite element approach have been proposed. Song *et al.* identified the pipe radius-to-wall thickness ratio (R/t) and welding heat input (Q) as the two principal parameters governing residual stress distribution in austenitic stainless steel welds.[16]

In this work, a structured study of residual stress measurements in austenitic stainless steel pipe girth welds covering a wide range of welding and geometry parameters are presented. The measured data are used to validate residual stress profiles predicted by an artificial neural network approach. Neutron diffraction and the contour method are employed for measuring newly manufactured girth-welded pipes, while historic data were predominantly measured using deep hole drilling (DHD). The DHD method is susceptible to plasticity induced errors and incremental deep hole drilling (iDHD) was proposed to mitigate this limitation.[17]

In this paper, we present (i) residual stress measurements in pipe welds having a range of welding and geometry parameters; (ii) development of an ANN predictive approach trained using residual stress measurements; (iii) validation of the residual stress profiles predicted by the trained ANN model; and (iv) critical evaluation of the ANN approach, identifying scope for further improvement.

II. MATERIAL DESCRIPTION

Six austenitic stainless steel pipe butt welds were fabricated to perform a characterization study of the residual stress distribution, and the data obtained were added to the measurement database of residual stress profiles from historic measurements. The geometry and chemical composition of the pipe butt welds are as follows:

1: A welded component 35 mm thick, 200 mm long, and 180 mm outer diameter (denoted as 'A') made of Esshete 1250 material (0.097 C, 0.45 Si, 6.73 Mn, 14.71 Cr, 9.38 Ni, 0.95 Mo, 0.28 V, 0.13 Cu, and balance Fe in wt pct).
2, 3: Two 25-mm-thick welds, 320 mm long and 250 mm OD (denoted as 'B' and 'C') made of austenitic stainless steel grade 316 L (0.02 C, 0.51 Si, 0.94 Mn, 16.7 Cr, 11.1 Ni, 2.0 Mo, and balance Fe in wt pct).
4, 5, 6: Three 12.7-mm-thick welds, 300 mm long and 265 mm OD represented as 'D,' 'E,' and 'F,' made from 316 steel made of austenitic stainless steel grade 316 L (0.02 C, 0.51 Si, 0.94 Mn, 16.7 Cr, 11.1 Ni, 2.0 Mo, and balance Fe in wt pct).

Welds having the same wall thickness and outer diameter were made using different electrical heat inputs to investigate the effect on the resulting residual stress distribution. All welds were received in the ''as-welded'' condition. The weldments were sectioned, polished, and etched (electrolytic using 5 pct oxalic acid at 6 V for 30 seconds) to reveal the weld beads and fusion boundaries. Two through-thickness lines are defined: the weld center line (WCL) which is the center line of the weld; and a heat-affected zone (HAZ) line passing through the extreme edge of the weld on the last capping pass side as shown in Figure 1(b).

III. RESIDUAL STRESS MEASUREMENT METHODS

Neutron diffraction and the contour method were chosen to measure residual stresses in the pipe girth welds because they have the capability of mapping stresses through the thickness of the components.

A. *Neutron Diffraction*

Neutron diffraction has been successfully applied to characterize the through-thickness residual stress distribution in austenitic stainless steel pipe welds.[18] In this work, the neutron diffraction studies were performed using the SALSA[19] diffractometer at the Institut Laue-Langevin (ILL), Grenoble, France. The crystallographic strain ε_{hkl} can be calculated from the lattice spacing (d_{hkl}) and stress-free reference parameter ($d_{0,hkl}$) for a particular set of hkl planes using the equation:

$$\varepsilon_{hkl} = \frac{d_{hkl} - d_{0,hkl}}{d_{0,hkl}}. \quad [1]$$

Determining accurate stress-free lattice parameters is crucial in neutron diffraction strain measurements as a small change can result in significant errors in the measured residual stress distribution. The stress-free

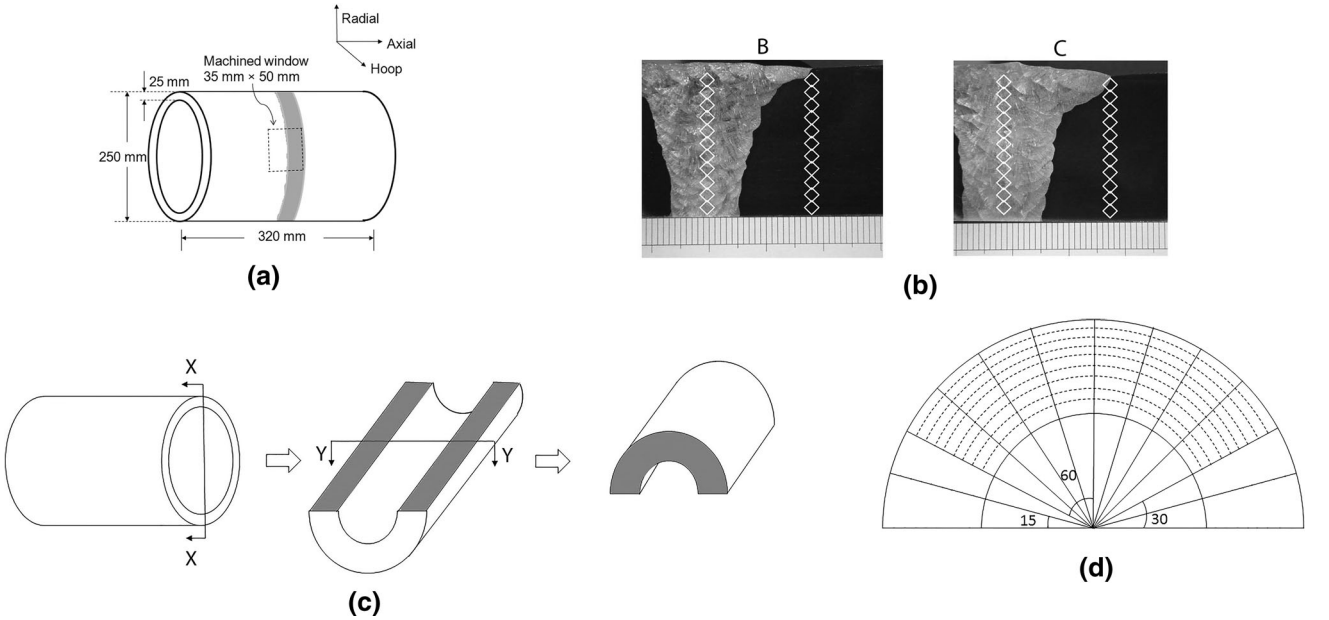

Fig. 1—Schematic illustration of neutron diffraction experiment (*a*) location of the plug of material used to extract stress-free samples. (*b*) Measurement locations of through-thickness profiles at weld center line and heat-affected zone. (*c*) The stages of the contour method to characterize hoop and axial stresses; first cut was undertaken along plane XX to map the hoop stresses and second cut along plane YY to determine stresses along the axial direction. (*d*) Extraction of through-thickness stress profiles from the 2D axial stress distribution: Through-thickness profiles are extracted every 15 deg in the clockwise direction and an averaged stress profile along the 120 deg segment from the maps of axial stresses.

lattice parameter is affected by changes in material chemistry, the presence of texture, large grains, and inter-granular strains. The neutron experiments in this study were conducted to measure the residual stress field of two of the welded pipes, denoted B and C. An access window of dimensions 35 mm × 50 mm was machined in each of the pipes (see Figure 1(a)) using a die-sink electro-discharge machining (EDM) process prior to the neutron diffraction measurements. Neutrons having a wavelength of 1.648 Å were chosen to give a diffraction angle of about 99 deg for the {311} set of lattice planes. This reflection was chosen for the stainless steel face-centered cubic crystal structure because it has low sensitivity to inter-granular strains arising from plastic strain. The neutron beam was collimated to give a nominal gage volume of $(2.3 \times 2.3 \times 2.3)$ mm^3 and each pipe was set up on the instrument hexapod stage to measure strain components in three orthogonal directions (axial, hoop, and radial). The array of measurement points at the WCL and HAZ of the two pipes B and C are shown in Figure 1(b). The measurement location was offset by approximately 90 deg from the weld start-stop location. LAMP (Large Array Manipulation Program) software was used to analyze the data obtained from the neutron diffraction experiments. Cubes of dimensions 5 mm × 5 mm × 5 mm, representative of the weld and HAZ metal, were wire EDM machined from the plug of material removed from each pipe (to create the access window required to reduce the path length of the neutrons through the steel). Stress free lattice parameters measured in these cubes were used to provide position-dependent reference lattice values based upon second-order polynomial interpolation.

The measured lattice strains in three orthogonal directions were converted to stress assuming a generalized Hooke's law with a crystallographic {311} Young's modulus of 187 GPa and Poisson's ratio of 0.30. The error bars plotted for the neutron measurements of stress represent the uncertainty of fitting a function to the peak shape and background of the diffracted data, and do not include other potential sources of error such as variations in the elastic modulus.

B. *Contour Method*

The contour method is not affected by composition changes, large grain size, and crystallographic texture that can compromise diffraction techniques. However, it is very sensitive to the quality of sectioning cut and, in certain cases, errors associated with plasticity caused by stress redistribution ahead of the wire during the cutting process.

1. *Hoop stress measurement*

The contour method can be applied to complex geometries such as welded pipes, but is more challenging than in flat plates. The one-step cutting method[20] was applied in the present work; that is, the pipe was sectioned by cutting along a radial-axial plane (Section XX in Figure 1(c)) with the aid of a specially designed clamping jig. Extensive cutting trials were first conducted on 300 series stainless steel material that replicated the pipe geometry for the purpose of choosing cutting parameters that gave the best cut surface finish. An Agie Charmille F440S wire EDM with a wire diameter of 0.25 mm made of brass was used with "skim" cut settings. Pilot holes (4 mm diameter) were

drilled 15 mm from one end of the pipe in an attempt to reduce opening of the cut flanks and thereby reduce the risk of introducing significant plasticity at the cut tip. The same cutting mode was used for all contour cuts but with minor modifications to the EDM parameters to account for the variation in wall thickness and geometry.

The surface profiles of the mating cut surfaces were measured using a coordinate measuring machine (CMM) on a 0.5 mm × 0.5 mm grid with a touch probe system fitted with a 3-mm-diameter ruby tip. The two cut surfaces of each half-pipe were measured relative to a common coordinate system in order to capture the distortion owing to release of through-wall hoop bending stresses (that self-equilibrate across the diameter of the pipe). The surface contours were measured in a temperature-controlled environment after the test component had been allowed to reach room temperature. The datasets corresponding to the cut surfaces of the half-pipe pairs were aligned by translation and rotation of one dataset, before mapping onto a common grid system followed by averaging to eliminate shear stress effects. The averaged data were then essentially cleaned to remove the outliers and smoothed using a cubic spline curve fitting algorithm. In order to avoid over-smoothing or loss of spatial resolution in areas of high stress gradients, the knot spacings of the interpolation splines were optimized following the procedure reported.[21] For each measured pipe, an undeformed 3D model of one half-pipe was created using ABAQUS finite element (FE) software based on the measured perimeters of the cut faces. Linear hexahedral-reduced integration elements (C3D8R) were used with a fine mesh of 1 mm size at the cut surfaces and progressively coarsened around the pipe circumference. The averaged normal displacements were used as boundary conditions to the cut faces and rigid body motion restrained by using three additional displacement constraints. A linear elastic FE analysis was finally carried out to back calculate the residual stresses present prior to the cut, assuming isotropic material properties.

2. *Axial stress measurement*

In the contour method, multiple cuts can be employed to measure more than one stress component. This approach[22] was implemented in the present work to map the distribution of axial residual stress, through the thickness and around the circumference, of three pipe welds A, B, and C. The procedure involved making a cut across the diametral-hoop plane (Section YY in Figure 1(c)) at the weld center line of one of the half-pipes created by the hoop stress measurement. In order to ensure a uniform cut and minimize cutting artifacts, formers were machined to fit closely around the outside and inside of the half-pipe. The surface deformation contours for these cuts were measured using a Zeiss Eclipse laser non-contact coordinate measuring machine with a point density spacing of 0.25 mm × 0.25 mm. The data analysis procedure employed was similar to the hoop stress measurement with additional steps implemented to account for the stress relaxation effects from the first cut. This was accomplished by applying the displacement boundary conditions applied to the FE model created for determining the hoop stresses.

IV. MODELING USING ARTIFICIAL NEURAL NETWORKS

A. *Training and Validation*

The ANN was implemented using a back-propagation algorithm[23] with a multi-layer perceptron structure consisting of two layers of weights. The two-layer network has universal approximation capabilities[24] and hence it is not essential to consider other network architectures. The training is undertaken in the MATLAB neural network toolbox[25] using a scaled conjugate gradient method[26] that is capable of providing faster convergence in pattern recognition problems. Figure 2 presents the architecture and flowchart describing the ANN approach. The use of a non-linear transfer function makes a network capable of storing non-linear relationships between the input and the output. A log-sigmoidal transfer function was used in the hidden layer and linear function in the output layer. Initializing the neural network weights with small random values can avoid premature saturation of the sigmoidal functions. The net output y from the output layer is represented by Eq. [2],

$$y = \sum_{j=1}^{H} w_k \log h \left[\sum_{i=1}^{4} w_{ji} p_i + b^{(1)} \right] + b^{(2)}, \qquad [2]$$

where w_{ji} is the weight matrix of the hidden layer, w_j the weight matrix of the output layer, $b^{(1)}$ the bias vector of the hidden layer, $b^{(2)}$ the bias vector of the output layer, i the number of input variables, and H is the number of hidden nodes. The number of neurons (n) in the hidden layer was iteratively optimized based on the root mean square error of the test and training data given by

$$RMSE = \sqrt{\frac{\sum_{z=1}^{M} (t_z - y_z)^2}{M}}, \qquad [3]$$

where t is the desired value, y the output, and M is the number of samples.

The weights are iteratively updated during the training based on the sum of squared error governed by Eqs. [4] through [6],

$$w_{ji}(n+1) = w_{ji}(n) + \eta(\delta_{ji} y_{ji}) + \lambda \Delta w_{ji}(n) \qquad [4]$$

$$\text{Error } \delta_k = (t_k - y_k) y_k (1 - y_k) \quad \text{for output neuron} \qquad [5]$$

$$\text{Error } \delta_{ji} = (t_{ji} - y_{ji}) y_{ji} \sum \delta_{ji} w_{ji} \quad \text{for hidden neurons,} \qquad [6]$$

where λ is the momentum factor and η is the learning rate.

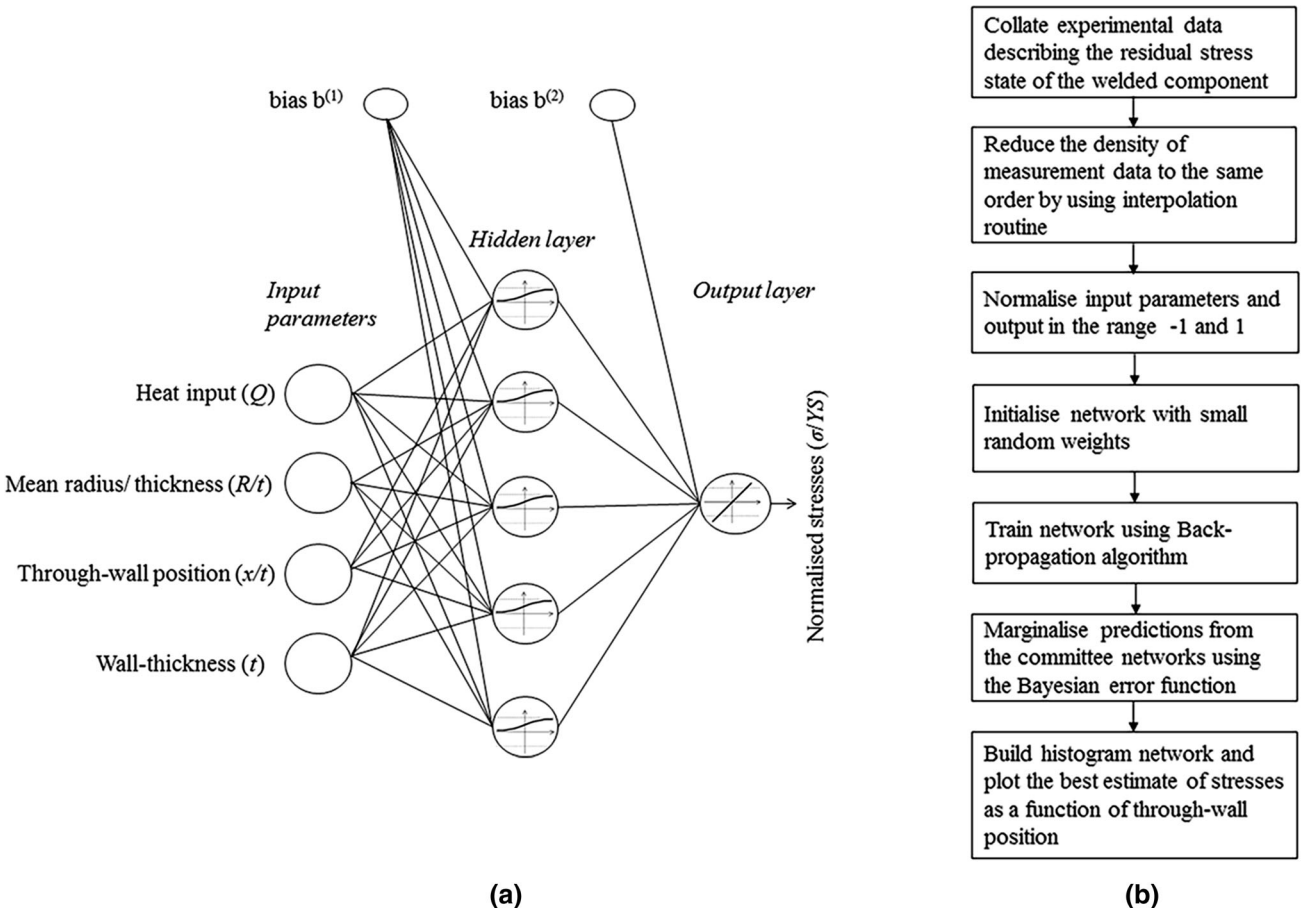

Fig. 2—(*a*) Artificial neural network architecture. (*b*) Flowchart describing the method in this study: x/t is the through-thickness position, Q the net heat input (kJ/mm), t wall thickness, R/t radius over thickness ratio, and YS is the yield strength at 1 pct proof stress. Log-sigmoidal function used in the hidden layer and linear function in the output layer.

Table I. Details of the Experimental Data Used for Training and Testing the ANN

Sample	Weld Process	Weld Heat Input, E (kJ mm^{-1})	R/t	Thickness, t (mm)	Weld Groove	Yield Strength of Parent Material, Y_p (MPa)	Yield Strength of Weld Material, Y_w (MPa)
A (Esshete 1250)	MMA	1.8	2.1	35	V-prep	370	564
B (316L)	TIG	1.0	4.5	25	V-prep	300	500
C (316L)	TIG	2.5	4.5	25	V-prep	300	500
D (316L)	TIG	0.7	10	12.7	V-prep	320	450
E (316L)	TIG	1.0	10	12.7	V-prep	320	450
F (316L)	TIG	1.2	10	12.7	V-prep	320	450
Weld C (316L)	SAW	2.2	25	15.9	double V	338	476
SP19 (316L)	MMA	1.4	10.5	19.6	outer J	272	446
OU20 (316L)	MMA	1.7	3.8	20	outer J	308	446
SP37 (316L)	MMA	2.1	5.3	37	outer J	328	446
S5VOR (316L)	MMA	2.4	2.8	65	outer J	328	446
S5Old (316L)	MMA	1.4	2.8	65	outer J	328	446
S5New (316L)	MMA	1.0	2.8	65	outer J	328	446
S5NG (316L)	TIG	2.2	3.0	62	narrow gap	328	446
RR (316L)	MMA	1.8	1.8	110	outer J	274	446

Test data were systematically excluded from the sample set used for training the ANN.

Table II. Summary of the Measurement Technique Used to Collate Experimental Data

Specimen Description	Axial Stress		Hoop Stress		Measurement Technique(s)
	WCL	HAZ	WCL	HAZ	
A	✔	X	✔	✔	CM
B	✔	✔	✔	✔	ND, CM
C	✔	✔	✔	✔	ND, CM
D	X	X	✔	✔	CM
E	X	X	✔	✔	CM
F	X	X	✔	✔	CM
Weld C	✔	X	✔	X	BRSL
SP19	✔	✔	✔	✔	ND
OU20	X	✔	X	✔	ND
SP37	✔	✔	✔	✔	DHD
S5VOR	✔	✔	✔	✔	DHD
S5Old	✔	X	✔	X	DHD
S5New	✔	✔	✔	X	DHD
S5NG	✔	✔	✔	✔	DHD
RR	✔	X	✔	X	DHD

BRSL: Block removal splitting and layering, ND: Neutron diffraction, CM: Contour method, DHD: deep hole drilling.

The geometry and welding conditions of the austenitic stainless steel girth welds collated over the last two decades including the measurements of the six girth welds reported in this work are summarized in Table I.

These data were obtained by diverse measurement techniques as part of the UK nuclear industry's research program. Details of each measurement technique used to characterize the residual stress distribution for a particular specimen can be found in Table II.

The training dataset contains deep hole drilling (DHD) measurements[27] that have higher measurement point density through the wall thickness than other techniques. This difference was compensated for in the model by reducing the density of DHD measurement points by a factor of 10 using the interpolation routine in MATLAB primarily to reduce computational time and to ensure the pattern is well captured in the data presented to the ANN. The measured residual stress data of the simulated stress profile are excluded from the training dataset; this is to test the ability of the ANN to generalize the pattern within the parametric space which did not form part of the training.

ANNs sometimes perform poorly when the 'weights' are reported to have implausibly large values in order to fit the details in the training data. The principle of Occam's razor, which states the importance of preferring simpler models over complex ones, is embodied in a Bayesian approach[28] which is particularly useful for weight regularization and marginalization of network output.

The generalization ability of the network is characterized by the error function $E(w)$ described as

$$E(w) = \beta Es + \alpha E_R \quad [7]$$

$$E_S = \frac{1}{2}\sum_{i=1}^{M}\{t - y(p,w)\}^2 \quad [8]$$

$$E_R = \frac{1}{2}\sum_{i=1}^{R}|wi|^2, \quad [9]$$

where β is the parameter controlling the variance in noise, α is the regularization coefficient, w is the weight vector. The regularization term favors small values of network weights and biases, thereby decreasing the susceptibility of the model to over-fit noise in the training data.

B. *Histogram Network*

In training, many different networks can be combined together to form an ensemble or "committee." This approach can be useful as it can lead to significant improvements in the predictions with small additional computational effort.[29] An ensemble of networks was created by running 250 independent training sessions. A histogram was developed to manage scatter within the neural network predictions and to provide a best estimate of the residual stresses. The 10 pct of predictions with the lowest Bayesian error was determined from the committee of 250 networks and a histogram of the output distribution was uniformly divided to express the model predictions as a distribution plot. The ANN prediction presented is intended to provide a reasonable estimate of through-thickness stress distributions. However, residual stresses evidently exhibit a high degree of scatter, especially in welds.[11] The use of a committee of networks to determine the optimum prediction by marginalization of the output is arguably an effective way of providing a reliable prediction interval of the estimated stress distributions.

V. RESULTS AND DISCUSSION

A. *Residual Stresses Measured Using the Contour Method*

The measured distribution of hoop stresses for specimens A, B, C, D, E, and F using the contour method are presented in Figure 3. The uncertainties from the measurements are judged to be in the order of ±30 MPa. It is common to observe peak stresses close to the yield strength of the material in the weld region.[27] Maximum tensile stresses as high as 500 MPa are observed at the top surface in the weld and compressive stresses of high magnitude (~400 MPa) at locations close to the weld root. The distributions of hoop residual stresses were found to vary not only with the geometry but also with the heat input used in welding, which matches well with the findings of previous studies.[7] Note that the specimen sets (B and C), and (D, E, and F) have the same geometry but were fabricated using different heat inputs and pass sequences. Moreover, the residual stresses in the vicinity of the weld are strongly affected by the shape of the fusion boundary as is evident from Figure 3. Interestingly, the contour method is able to capture the variation in stress across the weld and through the thickness in all cases. The stress distributions on the top and bottom cut faces of each pipe are almost symmetrical for all the pipe welds, which gives confidence in the contour measurement technique implemented. The minor stress distribution differences that exist are likely to be associated with weld lay-up variations as these samples were welded using the arc processes and are real variations around the circumference.

Figure 4 illustrates maps of axial stress measured by contour method in specimens A, B, and C. Peak tensile stresses of magnitude 350 MPa and compressive stresses

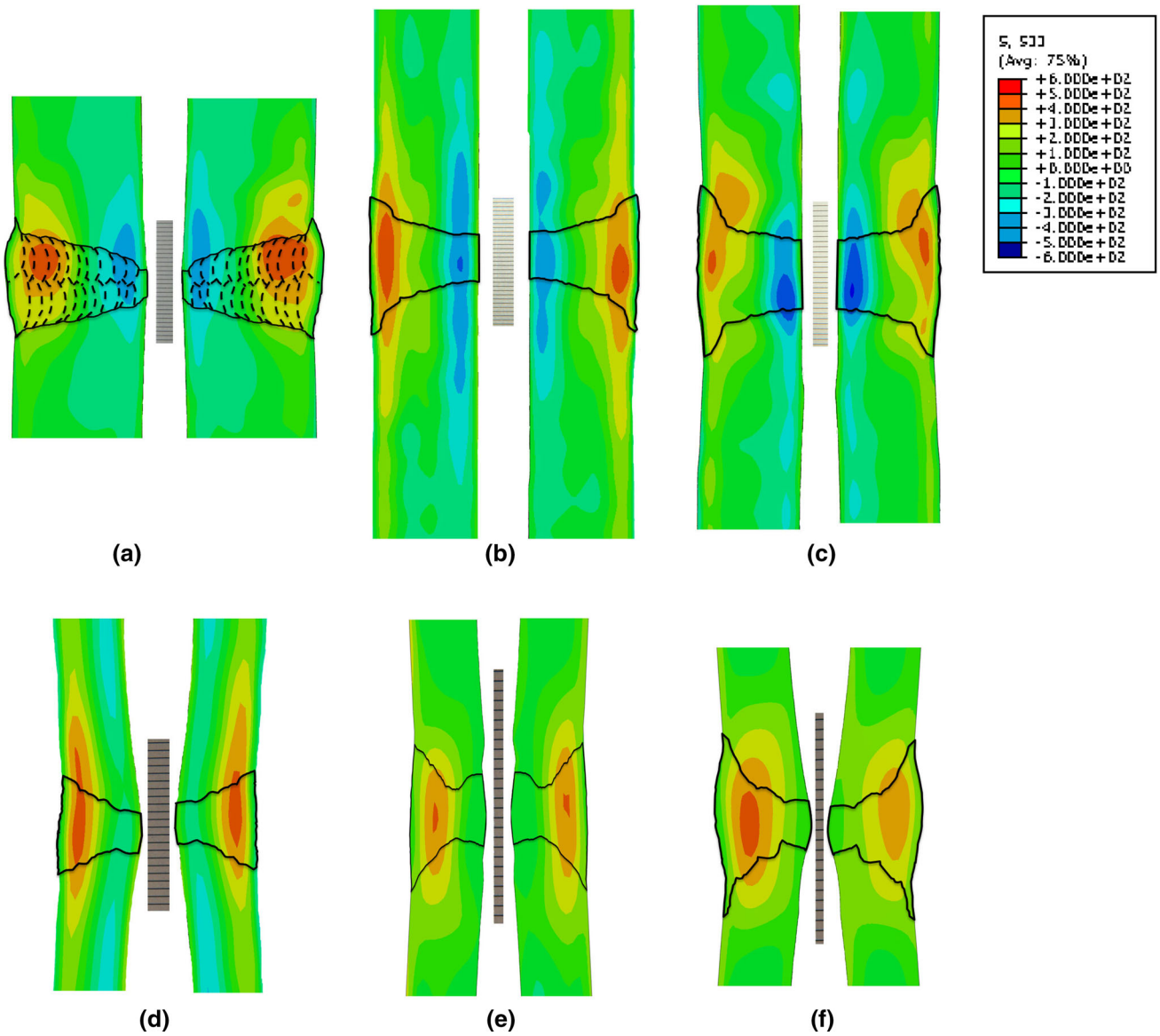

Fig. 3—Hoop stress maps measurements determined using the contour method in girth-welded pipes A, B, C, D, E, and F.

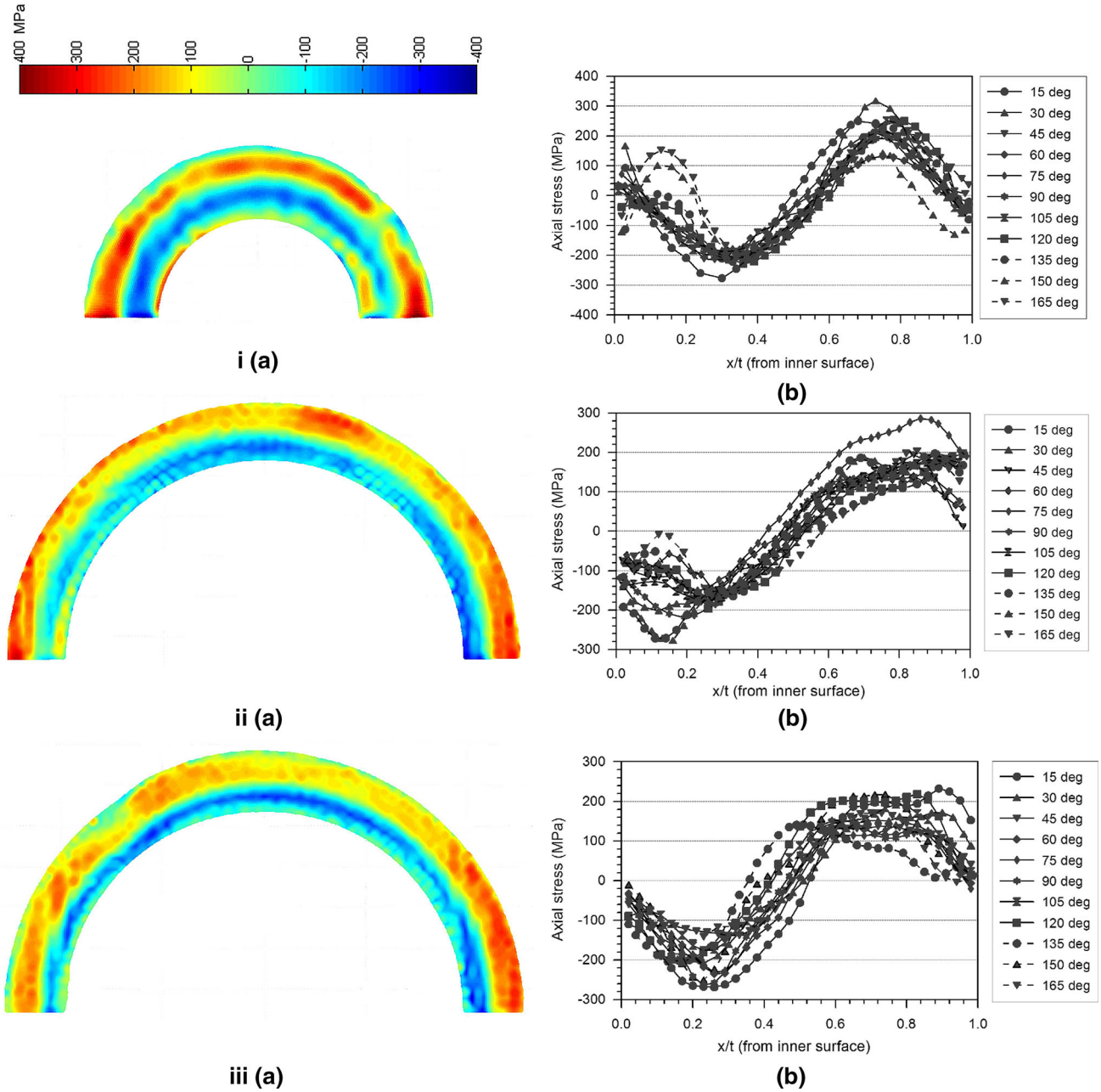

Fig. 4—Two-dimensional axial stress maps and through-thickness stress profiles at various locations using the contour method in specimens A—*i*(*a*) and (*b*), B—*ii*(*a*) and (*b*), and C—*iii*(*a*) and (*b*).

close to −300 MPa are observed in weld A (Figure 4(a)). The variation in axial residual stresses around the circumference of the weld is significant and associated with the finite length, geometry, and welding conditions of individual weld beads. Several through-thickness profiles at angles 15, 30, … 165 deg in the clockwise direction plus an averaged stress profile along the 120 deg segment are extracted from the maps of axial stresses as shown in Figure 1(d). This measurement is of high significance because it demonstrates that the through-wall axial residual stress profile can be substantially different depending upon its location around the circumference and relationship to the local weld lay-up; for example, the maximum tensile stress between −15 and 150 deg varies by 300 MPa close to the inside surface. Similar large variations around the circumference are observed in pipe welds B and C made using a TIG process, see Figures 4ii(b) and iii(b). This evidence illustrates one of the origins of "innate scatter of residual stresses."[11] It also suggests how a line profile cannot be used to characterize the local through-wall residual stress distribution in a pipe weld, and the value of providing a scatter band using the ANN is therefore emphasized. Overall, the results demonstrate how well the contour method can resolve complex hoop and axial residual stress fields in thick section pipe girth welds.

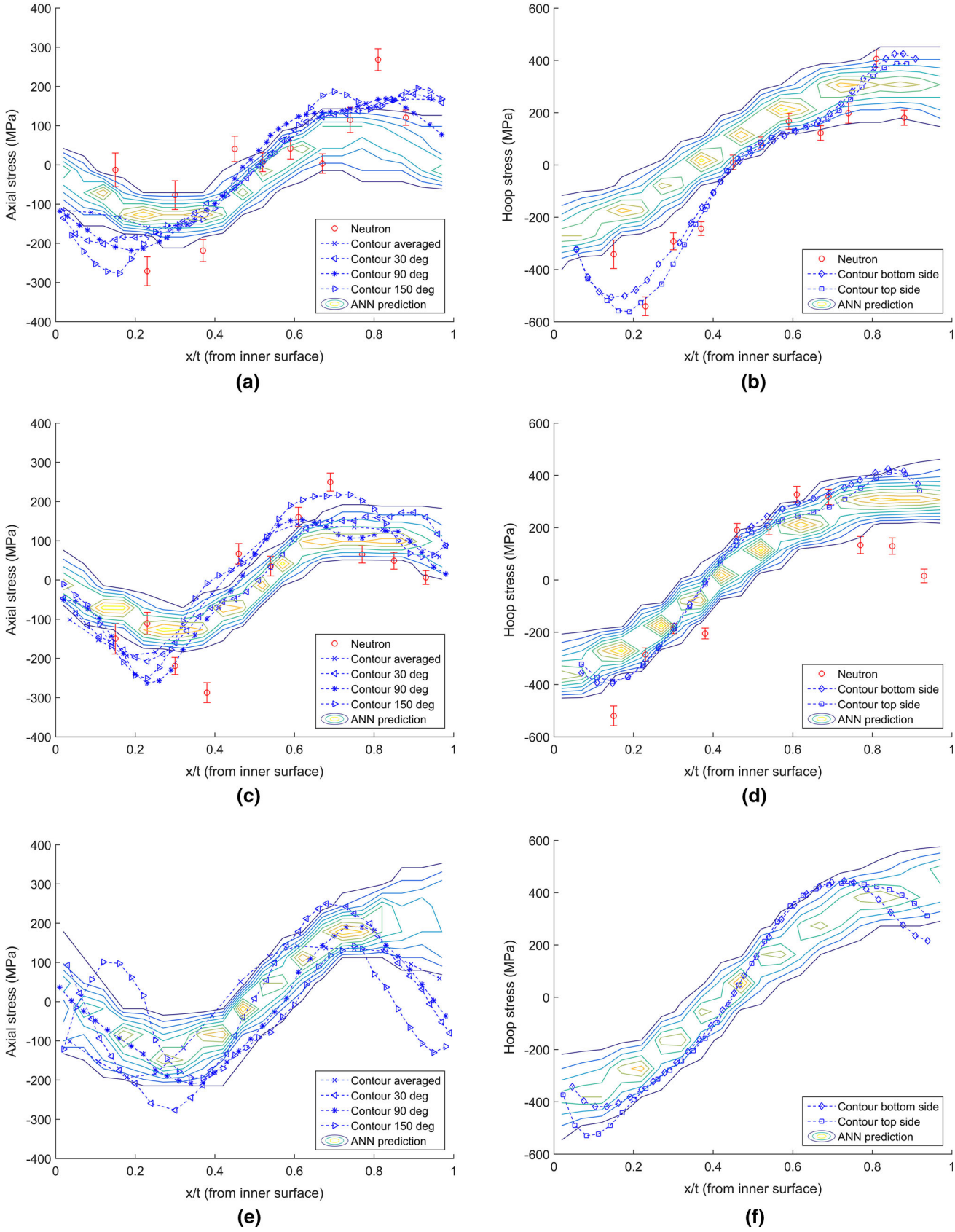

Fig. 5—Comparison of through-thickness profiles using neutron diffraction, contour method, and ANN prediction in the axial (left) and hoop (right) direction at the weld center line in specimens B—(*a*) and (*b*), C—(*c*) and (*d*), and A—(*e*) and (*f*), respectively.

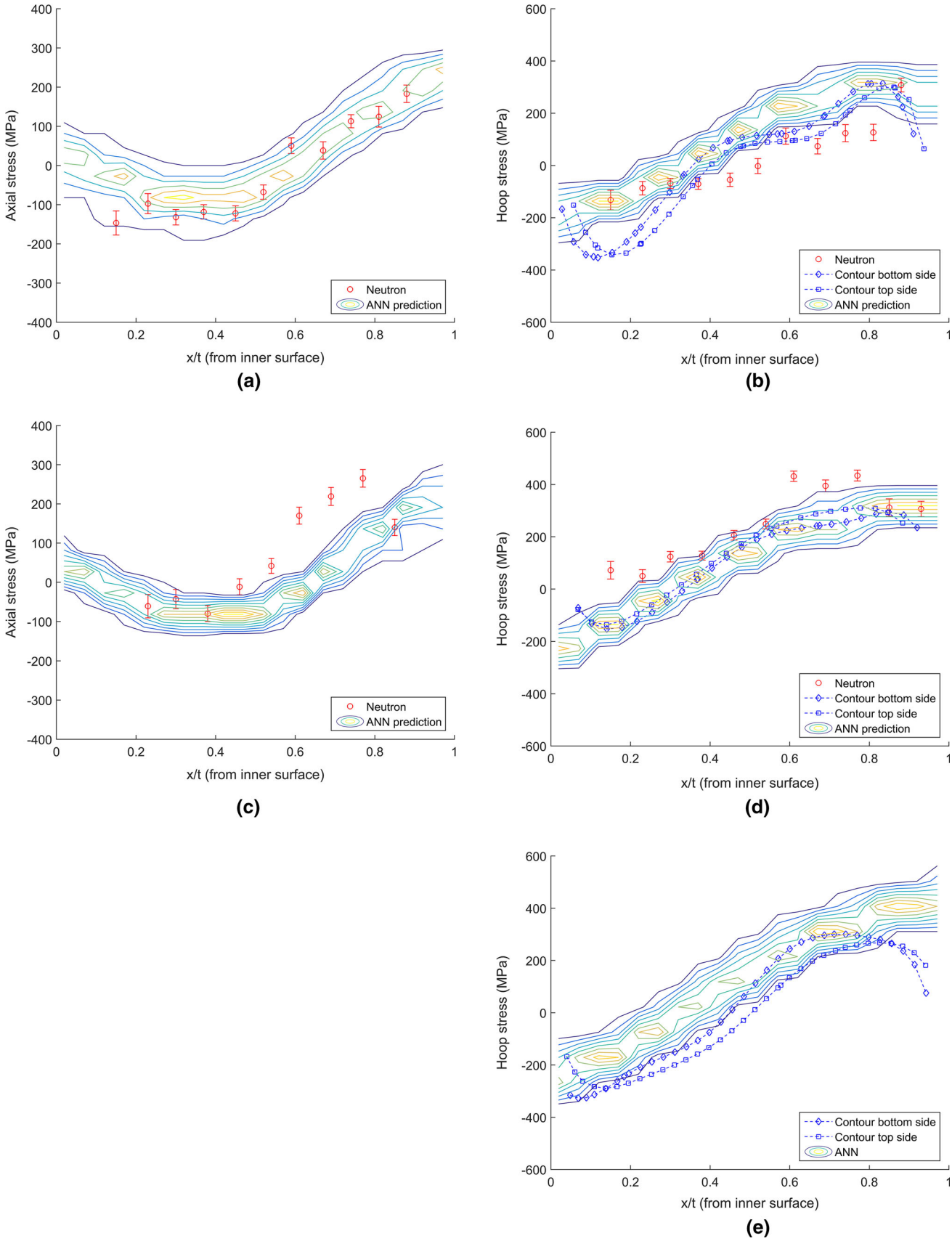

Fig. 6—Comparison of through-thickness profiles using neutron diffraction, contour method, and ANN prediction in the axial (left) and hoop (right) direction at the heat-affected zone in specimens B—(*a*) and (*b*), C—(*c*) and (*d*), and A—(*e*), respectively.

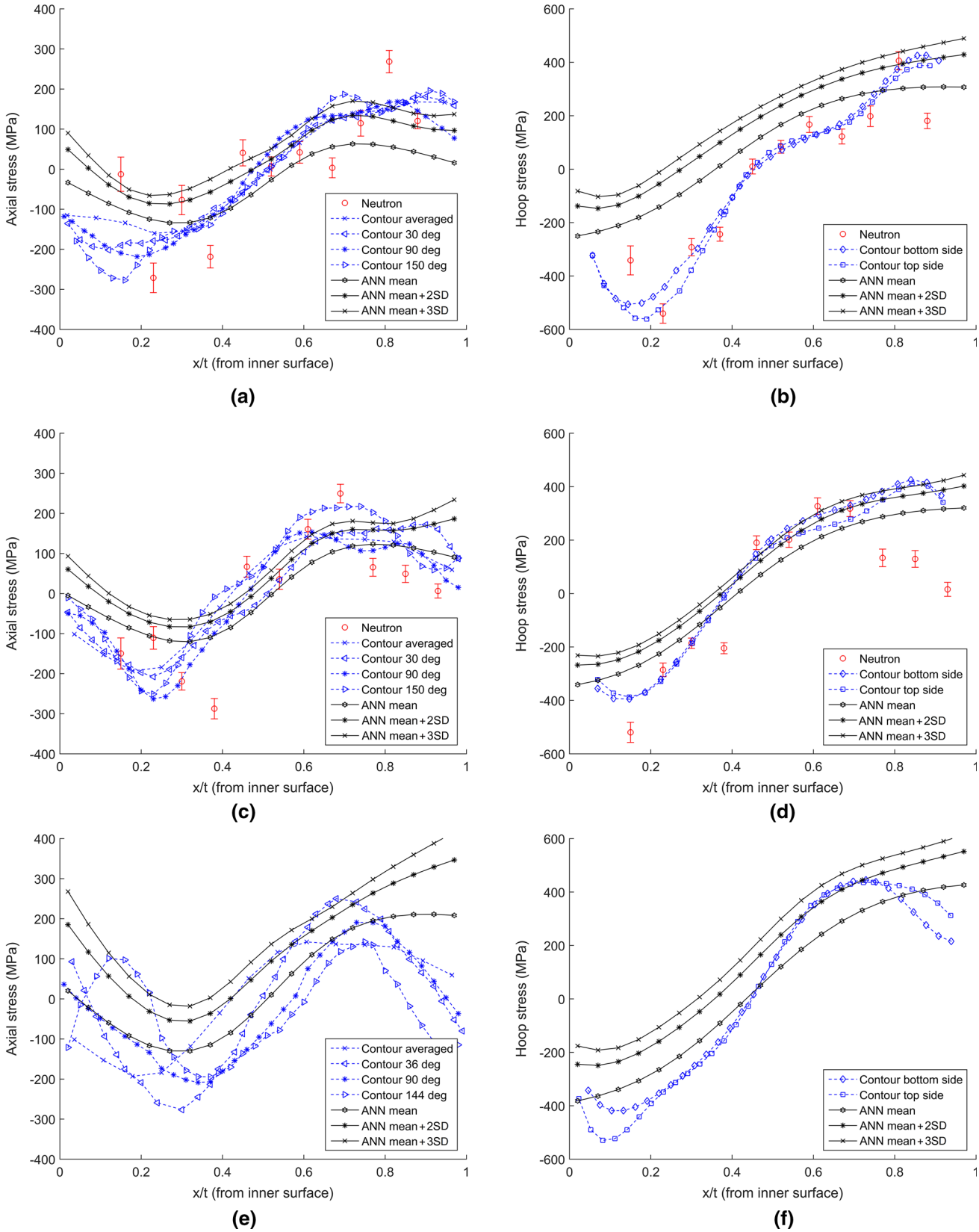

Fig. 7—Comparison of measured through-thickness profiles with the ANN mean prediction, ANN mean + 2SD, and ANN mean + 3SD in the axial (left) and hoop (right) direction at the weld center line in specimens B—(*a*) and (*b*), C—(*c*) and (*d*), and A—(*e*) and (*f*), respectively.

B. *Comparison of Through-Thickness Residual Stress Profiles*

Residual stress profiles predicted by the ANN at the weld center line of pipes A, B, and C are compared with the neutron and contour method measurements in Figure 5. In Figure 5(a), the ANN prediction is in reasonable agreement with the contour method measurements obtained at different locations around the circumference, whereas the neutron measurements imply the presence of higher tensile stress close to 280 MPa at $x/t = 0.8$. Note the ANN prediction is intended to provide a best estimate of stresses and may not always be able to capture the scatter in residual stresses evidenced in the contour measurement. However, it is highly desirable to be able to predict the peak tensile stresses measured using experimental techniques: under-prediction of stresses in any case is considered to be a weakness of the data-based approach.

In Figure 5(b), the prediction is compared with the hoop stress measurements for sample B. Very good agreement is seen between the neutron and the contour method measurements. However, there is a discrepancy of about 300 MPa between the ANN prediction and measurements near to the inside surface. Residual stresses of magnitude close to 600 MPa in compression were observed in the hoop direction of sample B that were not evident in any of the training data profiles. In Figure 5(c), the ANN prediction tends to under-predict the stresses in specimen C measured by neutron diffraction and contour method in the region $x/t = 0.4$ to 0.7. The prediction is slightly better in the hoop direction considering the agreement with the contour method measurements. The ANN prediction for the axial stresses in pipe A is unable to capture the sharp variation of stresses approaching the outer surface. In this case, the scatter among the measurements is higher and a difference of more than 200 MPa is seen at the outer diameter. However, the prediction agrees reasonably well with the measurements made by the contour method in the hoop direction for pipe A (see Figure 5(f)). In general, the ANN prediction is unable to capture high stress gradients near the surface despite the presence of similar patterns in the training data and this may be regarded as a limitation of the present approach.

Similar comparisons for residual stress profiles in the heat-affected zone (HAZ) are presented in Figure 6. There are no contour measurements in the axial direction at the HAZ location and the prediction is compared solely with neutron measurements. The measured axial stress profiles seem to be in fair agreement with the prediction in specimen B (Figure 6(a)), but the model under-predicts the stresses measured using neutron diffraction in specimen C over the through-wall position range $x/t = 0.5$ to 0.8 (see Figure 6(c)). The hoop stress experimental data for specimens B, C, and A (Figures 6(b), (d), and (e), respectively) are in good agreement with the ANN prediction. Overall, the ANN was capable of providing predictions for the various cases considered. The change in pattern for the different predictions demonstrates that the ANNs can capture the non-linear pattern in the data trained using the input parameters employed in this study.

C. *Critical Evaluation of the ANN Method*

The differences in residual stress profiles measured using neutron diffraction and the contour method in Figures 5 and 6 are examined. It was found that there was a general qualitative agreement between the two measurement techniques particularly at measurement locations having peak tensile stresses. However, the magnitude of the measured residual stress distributions showed discrepancies and there are numerous occasions where neutron diffraction measurements have implied higher residual stresses than those obtained using the contour method. This is due to the inherent differences associated with the measurement capabilities of both techniques.[7] It is important to note that the training dataset comprised mostly contour method and DHD measurement data, and under-prediction of stresses by the ANN in many cases (for example see Figures 5(a) and (c), 6(c), and (d)) could be related to the lack of neutron diffraction data in the learning process. Another possible explanation for under-prediction is linked with the extensive amount of deep hole drilling (DHD) data in the training dataset. The DHD technique is capable of measuring two in-plane components of the stress tensor as a function of distance through the thickness. However, the method is not very reliable where the stresses exceed about 50 pct of the yield strength of the material.[30] As a consequence, the incremental deep hole drilling (IDHD) technique was later proposed[16] as a refinement to mitigate the limitation of measuring high-magnitude residual stresses close to the yield strength and to account for plasticity effects associated with the conventional DHD method. The DHD method is believed to have inferred significantly lower residual stresses both in tensile and compressive direction, and hence would have caused higher prediction inaccuracies in the trained ANN model.

A conservative estimate of residual stress distributions is often required for structural integrity assessments. It is not advisable to use a model that may under-predict the experimental measurements by a large margin. As illustrated in Figure 4, the through-wall residual stress distribution in a pipe weld can vary significantly depending upon location around the circumference and the influence of the weld bead lay-up. The scatter band provided by the ANN can effectively be used to quantify the residual stress variability across the circumference. To demonstrate the robustness of the ANN approach, the experimental measurements along the weld center line are compared with the ANN mean profile (mean of best 10 pct of predictions), ANN mean + 2 Standard deviation (denoted by ANN mean + 2SD), and ANN mean + 3 Standard deviation (denoted by ANN mean + 3SD) each covering 95.5 and 99.7 pct of the prediction data in the ANN distribution plot. In Figure 7(a), the 3SD profile reasonably bounds all the measurements except one neutron data point and a few contour measurements close to the outer surface.

In the hoop direction (see Figure 7(b)), both the 2SD and 3SD profiles effectively bound all of the measurement points. The ANN 3SD profile is not conservative and fails to bound measurements from the through-wall position range $x/t = 0.3$ to 0.8 in the axial direction of specimen C (see Figure 7(c)). Nevertheless, the 3SD profile bounds all measurements in the remaining three cases (Figure 7(d), (e), and (f)). The results illustrated in Figure 7 suggest that in spite of the limitations in the training data used, the ANN is capable of providing realistic bounding estimates of residual stresses compared with the experimental measurements, as slight over-prediction is permissible if experimental results fall below the prediction band. In fracture assessments, such bounding estimates of through-thickness stress profiles are used to evaluate the stress intensity factor or the elastic crack driving force. The crack driving force parameter that is generally conservative in nature can be evaluated consequently based on a set of conditions (such as crack length, shape, and loading conditions) and are directly used in fracture assessments of safety-critical components.

Predicted residual stress profiles have been found to be in reasonable correlation with experimental measurements by using the training data obtained from diverse experimental measurements that cover a wide range of welding conditions and geometries. The quantitative agreement showed good performance against unseen data within the bounds of the input parameter space. Moreover, the ANN approach was successful in identifying non-linear patterns in both the weld center line and heat-affected zone residual stress profiles. The ANN method is suitable for application where a best estimate of stresses or a bounding profile is required. However, this is subjected to the caveat that adequate sensitivity studies are undertaken prior to the application and appropriate safety margins are included. Additionally, it is not possible to assign any rank or preferential treatment to the measured data used in training. The ANN approach has also not been very effective in capturing high stress gradients and stresses close to the outer surface. This could be resolved by including a series of round robin experiments comprising neutron diffraction and surface measurements. In contrast, the information required to train the neural network is not onerous and takes into account all the key parameters such as geometry and the heat input associated with welding. However, the application of the model requires the construction of an improved database with greater neutron diffraction, contour method, and surface measurements covering all regions of the process parameter space.

VI. CONCLUSIONS

1. A data-based approach using an artificial neural network has been developed that can characterize the through-wall distribution of residual stresses as a function of welding heat input and geometry in austenitic stainless steel pipes. The ANN approach has been validated by comparing predicted profiles with experimental measurements made using neutron and contour method measurements.
2. The contour method was able to resolve high stress gradients in the axial and hoop direction for all the characterized samples. Significant scatter of more than 200 MPa was observed within the measured results at the weld center line in the axial direction and are associated with the geometry and welding conditions of individual weld beads.
3. A structured study of through-thickness profiles was undertaken to identify trends in welding-induced residual stresses in austenitic stainless steel pipes. The ANN has been successful in learning the non-linear patterns associated with the residual stress profiles in the weld center line and heat-affected zone. However, the construction of an improved database by including a series of round robin experiments comprising neutron diffraction, contour method, and surface measurements covering all regions of the process parameter space is recommended for application of the ANN model.
4. The scatter band provided by the ANN can quantify the residual stress variability across the circumference. A profile based on the ANN mean + 3 standard deviations is capable of bounding measured residual stress profile measurements in most cases along the weld center line and could be employed as a surrogate method to evaluate the stress intensity factor in structural integrity assessments. However, this is subjected to the caveat that adequate sensitivity studies are undertaken prior to the application, and that appropriate safety margins are included.

ACKNOWLEDGMENTS

The authors are grateful for funding received from EDF Energy, AMEC Power and Process Europe, and the Lloyd's Register Foundation. The award of neutron beamtime by the Institut Laue-Langevin (ILL) is also gratefully acknowledged. Michael Fitzpatrick and Jino Mathew are funded by the Lloyd's Register Foundation (LRF), a charitable foundation helping to protect life and property by supporting engineering-related education, public engagement, and the application of research. Pete Ledgard and Stan Hiller from the Open University, and Paul English from the University of Manchester are also acknowledged for their assistance for carrying out the experiments.

REFERENCES

1. P.J. Withers: *Rep. Prog. Phys.*, 2007, vol. 70, pp. 2211–64.
2. R6 Revision 4: *Assessment of the integrity of structures containing defects*, Gloucester, 2009.
3. GS Schajer: *Practical Residual Stress Measurement Methods*, Wiley, Chichester, 2013, pp. 6–24.

4. M.T. Hutchings, P.J. Withers, T.M. Holden, and T. Lorentzen: *Introduction to the Characterization of Residual Stress by Neutron Diffraction*, Taylor and Francis, London, 2005, pp. 149–99.
5. M.B. Prime: *J. Eng. Mater. Technol.*, 2001, vol. 123, pp. 162–68.
6. M.C. Smith, P.J. Bouchard, M. Turski, L. Edwards, and R.J. Dennis: *Comput. Mater. Sci.*, 2012, vol. 54, pp. 312–28.
7. W. Woo, G.B. An, E.J. Kingston, A.T. DeWald, D.J. Smith, and M.R. Hill: *Acta Mater.*, 2013, vol. 61, pp. 3564–74.
8. P.J. Withers, M. Preuss, A. Steuwer, and J.W.L. Pang: *J. Appl. Crystallogr.*, 2007, vol. 40, pp. 891–904.
9. F. Hosseinzadeh, J. Kowal, and P.J. Bouchard: *J. Eng.*, 2014, pp. 1–16, DOI:10.1049/joe.2014.0134.
10. B. Ahmad and M.E. Fitzpatrick: *Metall. Mater. Trans. A*, 2016, vol. 47A, pp. 301–13.
11. P.J. Bouchard: *Int. J. Press. Vessels Pip.*, 2008, vol. 85, pp. 152–65.
12. C.M. Bishop: *Neural Networks for Statistical Pattern Recognition*, Oxford University Press, Oxford, 1994, pp. 1–27.
13. H.K.D.H. Bhadeshia, R.C. Dimitriu, S. Forsik, J.H. Pak, and J.H. Ryu: *Mater. Sci. Technol.*, 2009, vol. 25, pp. 504–10.
14. İ. Toktaş and A.T. Özdemir: *Expert Syst. Appl.*, 2011, vol. 38, pp. 553–63.
15. M.G. Na, J.W. Kim, D.H. Lim, and Y.-J. Kang: *Nucl. Eng. Des.*, 2008, vol. 238, pp. 1503–10.
16. S. Song, P. Dong, and X. Pei: *Int. J. Press. Vessels Pip.*, 2015, vols. 126–127, pp. 58–70.
17. A.H. Mahmoudi, S. Hossain, M.J. Pavier, C.E. Truman, and D.J. Smith: *Exp. Mech.*, 2009, vol. 49, pp. 595–604.
18. R.D. Haigh, M.T. Hutchings, J.A. James, S. Ganguly, R. Mizuno, K. Ogawa, S. Okido, A.M. Paradowska, and M.E. Fitzpatrick: *Int. J. Press. Vessels Pip.*, 2013, vol. 101, pp. 1–11.
19. T. Pirling, G. Bruno, and P.J. Withers: *Mater. Sci. Eng. A*, 2006, vol. 437, pp. 139–44.
20. F. Hosseinzadeh and P.J. Bouchard: *Exp. Mech.*, 2012, vol. 53, pp. 171–81.
21. M.B. Prime, R.J. Sebring, J.M. Edwards, D.J. Hughes, and P.J. Webster: *Exp. Mech.*, 2004, vol. 836, pp. 1–10.
22. P. Pagliaro, M.B. Prime, H. Swenson, and B. Zuccarello: *Exp. Mech.*, 2009, vol. 50, pp. 187–94.
23. D.E. Rumelhart, G.E. Hinton, and R.J. Williams: *Nature*, 1986, vol. 323, pp. 533–36.
24. K. Hornik, M. Stinchcombe, and H. White: *Neural Netw.*, 1989, vol. 2, pp. 359–66.
25. MATLAB: *MATLAB and Neural Network Toolbox Release 2012a*, The MathWorks Inc., Natick, MA, 2012.
26. M.F. Møller: *Neural Netw.*, 1993, vol. 6, pp. 525–33.
27. P.J. Bouchard: *Int. J. Press. Vessels Pip.*, 2007, vol. 84, pp. 195–222.
28. D.J.C. Mackay: PhD thesis, California Institute of Technology, 1991.
29. RJ Mammone: *Artificial Neural Networks for Speech and Vision*, Chapman & Hall Inc., New york, 1993, pp. 126–42.
30. S. Hossain: PhD thesis, University of Bristol, 2005.